CDF/PUB/TOP/CDFR/11033

Updated Measurement of the Single Top Quark Production Cross Section in the Missing Transverse Energy plus Jets Topology in $p\bar{p}$ Collisions at $\sqrt{s} = 1.96$ TeV

The CDF Collaboration[1]

[1] *URL http://www-cdf.fnal.gov*

(Dated: May 9, 2014)

Abstract

An updated measurement of the electroweak single top quark production cross section is presented using the full CDF data set corresponding to 9.5 fb^{-1} of integrated luminosity. The selected data sample is composed of events with an imbalance in the total transverse energy, b-tagged jets, and no identified leptons ($\not\!\!E_T b\bar{b}$). A combined s- and t-channel electroweak single top quark cross section of $3.53^{+1.25}_{-1.16}$ pb is measured and a lower limit on $|V_{tb}|$ of 0.63 is obtained at the 95% credibility level. The total uncertainty of this measurement is 40% less than that of the previous CDF measurement, which used one quarter of the full CDF data set. These measurements are combined with previously reported CDF results obtained from events with an imbalance in total transverse momentum, b-tagged jets, and exactly one identified lepton ($\ell\nu b\bar{b}$). An s- and t-channel electroweak single top quark cross section of $3.02^{+0.49}_{-0.48}$ pb and a lower limit on $|V_{tb}|$ of 0.84 at the 95% credibility level are obtained for the combination.

PACS numbers: 14.65.Ha, 13.85.Ni, 12.15.Hh

The observation of electroweak single top quark production at the Tevatron was a significant achievement for the CDF and D0 experiments [1], allowing precise measurements of the cross section at a hadron collider, and the ability to place an upper limit on the Cabibbo-Kobayashi-Maskawa (CKM) [2] matrix element magnitude $|V_{tb}|$ due to the direct coupling of the b quark with the singly-produced top quark.

The standard model (SM) prediction for the combined s- and t-channel electroweak single top quark production cross section has been calculated to next-to-next-to-leading order: $\sigma_{\rm SM}^{s+t} = 3.15 \pm 0.36$ pb [3, 4], excluding the contribution from the tW production mode, which is expected to be negligible in this final state [5]. The primary sensitivity to measuring this quantity is usually obtained from events where the W from the $t \to Wb$ process [6] decays leptonically to an $\ell\nu$ lepton pair (where ℓ represents either an electron e or muon μ) with a pair of jets, one of which is "b-tagged" or identified as likely having originated from a bottom quark. This sample of events (hereafter the "$\ell\nu b\bar{b}$" sample) provides a distinct signature against backgrounds produced by the strong force (QCD multijet or "MJ" background), which contain no leptons.

A complementary method in measuring the electroweak single top quark cross section is through events in the final state that contain two or three jets and significant imbalance in the total transverse energy $\not\!\!E_T$ [7], which results from the leptonic decay of the W boson, where the lepton has not been identified due to reconstruction or acceptance effects. Although MJ events comprise the dominant background in this final state (hereafter the "$\not\!\!E_T b\bar{b}$" analysis or sample), the requirement of significant $\not\!\!E_T$ greatly suppresses the MJ background. In addition, this search has sensitivity to events where the W boson decays via $W^- \to \tau^- \bar{\nu}_\tau$, and the τ^- decays hadronically in the form of a reconstructed jet.

The first CDF measurement of electroweak single top quark production in the $\not\!\!E_T b\bar{b}$ final state was performed with a dataset corresponding to an integrated luminosity of 2.1 fb^{-1} [8]. This article presents a new measurement using the full CDF data set (9.5 fb^{-1}). All the techniques developed in the search for s-channel electroweak single top quark production in the $\not\!\!E_T b\bar{b}$ sample [9] are exploited in this update. The strategy for this analysis is described in Ref. [9]. Important aspects of the analysis methodology are restated here for completeness. The results of this analysis and those of the most recent $\ell\nu b\bar{b}$ analysis [10] are then combined to obtain a more precise measurement of the electroweak single top cross section and to place a lower limit on the CKM matrix element magnitude $|V_{tb}|$.

Events are selected in which the calorimeter missing transverse energy $\not\!\!E_T$(cal) satisfies a minimum online trigger threshold of at least 45 GeV, or 35 GeV when at least two jets are present. In the offline analysis, events are accepted in which the reconstructed missing transverse energy $\not\!\!E_T$ is at least 35 GeV. Raw jet energies are corrected to account for irregularities in calorimeter response, energy lost outside the jet cone, and underlying event dynamics [11]. The jet energy scale and resolution, as well as the $\not\!\!E_T$ resolution, are further improved by incorporating corrections based on track-momentum measurements [12].

Each event is required to have at least two leading-E_T jets with transverse energies, $E_T^{j_1}$ and $E_T^{j_2}$, that satisfy $25 < E_T^{j_1} < 200$ GeV and $20 < E_T^{j_2} < 120$ GeV, respectively. Additionally, both leading-E_T jets are required to be reconstructed within the silicon detector acceptance, corresponding to pseudorapidity requirements of $|\eta| < 2$ for both jets, with one of them satisfying $|\eta| < 0.9$. Events with three jets are considered if the third-most energetic jet satisfies $15 < E_T^{j_3} < 100$ GeV and $|\eta| < 2.4$, while event with four or more jets are rejected. To discriminate against MJ background, the angular separation between the leading-E_T jets must satisfy $\Delta R > 0.8$. Events that satisfy these requirements are labeled "pre-tagged" events.

To suppress light-flavor MJ background, at least one of the leading-E_T jets is required to be b-tagged, which is achieved using the HOBIT algorithm [13]. The HOBIT algorithm assigns each jet a value between 0 and 1; jets with a HOBIT value between 0.72 (0.95) and 0.95 (1) are considered to be loosely (tightly) tagged. As two b quarks are present in the electroweak single top final state, events are separated into three categories based on how many jets are successfully identified as having originated from a b quark: events with only one tightly tagged jet and no other tag (1T), events with two tightly tagged jets (TT), and events with one tightly tagged jet and one loosely tagged jet (TL). Events are further classified according to the total number of jets, leading to six event subsamples that are analyzed separately to enhance sensitivity and to help separate s-channel electroweak single top quark production, enhanced in the double tagging categories, from the t-channel production, which is enhanced in the single tagging categories.

All events that satisfy the above kinematic and b-tagging criteria are separated into two samples. Events that contain no identified leptons comprise the preselection sample, which includes events in the signal region, which is defined below. Events that contain at least one identified charged electron or muon comprise the electroweak sample, which is used to

validate the background modeling derived for this analysis.

Most physics processes are modeled using Monte Carlo simulation programs. The electroweak single top samples are modeled using the POWHEG generator [14]. Backgrounds from V+jets (where V represents a W or Z boson) and $W + c$ processes are modeled using ALPGEN [15] with showering simulated by PYTHIA [16]. Events from diboson (VV), strongly produced $t\bar{t}$ (assuming a top-quark mass of 172.5 GeV), and associated Higgs boson production with a W or Z boson (VH) are simulated using PYTHIA. Two remaining backgrounds include contributions from events with falsely-tagged jets ("electroweak mistags") and MJ events.

The electroweak mistag samples are modeled by weighting V+jets and diboson-simulated events by mistag probabilities, derived from dedicated data samples [17]. The dominant background in the $\not\!\!E_T b\bar{b}$ sample, however, originates from the MJ background. To model this background, the same data-driven method described in Ref. [18] is used: the MJ background is derived by weighting each pretagged data event by a tag-rate probability derived from a MJ-dominated data sample.

At this stage of the analysis, placing simple requirements on kinematic event properties is not sufficient to separate the electroweak single top signal from the background. A series of multivariate discriminants that take advantage of nontrivial variable correlations are therefore employed to optimize suppressing the MJ background and to separate the electroweak single top signal from the remaining backgrounds.

The dominant background in the preselection sample corresponds to that of MJ events. To discriminate against this background, the same $\mathrm{NN_{QCD}}$ multivariate discriminant that was developed in the $\not\!\!E_T b\bar{b}$ s-channel electroweak single top search [9] is used. The $\mathrm{NN_{QCD}}$ algorithm was trained including several kinematic, angular, and topological variables whose shapes are different between MJ backgrounds and single top signal.

All events that satisfy a minimum $\mathrm{NN_{QCD}}$ threshold requirement populate the signal region, in which the dominant backgrounds are from MJ production, V+heavy-flavor jets events, and $t\bar{t}$ events. Events that do not meet the minimal $\mathrm{NN_{QCD}}$ threshold are used to validate the background prediction with the data. From this validation, multiplicative correction factors ranging from 0.7 to 0.9 are derived for each of the 1T, TL and TT MJ predictions. These corrections are applied to the appropriate MJ background normalization so that the data and the total predicted background normalizations are in agreement.

For all events contained in the signal region, two additional discriminants are developed that further exploit the differences in kinematic properties between (a) the signal and the V+jets background and (b) the signal and $t\bar{t}$ background processes. The first discriminant $\mathrm{NN}_{V\mathrm{jets}}$ is trained using simulated t-channel electroweak single top quark events for the signal sample and MJ-modeled events that satisfy the requirement on $\mathrm{NN}_{\mathrm{QCD}}$, for the background sample. The second discriminant $\mathrm{NN}_{t\bar{t}}$, is trained to separate t-channel electroweak single top quark from $t\bar{t}$ production, again using simulated t-channel electroweak single top quark events for the signal but simulated $t\bar{t}$ for the background. The values of these two discriminants (both supporting values between 0 and 1) are then combined in quadrature resulting in an overall discriminant called $\mathrm{NN}^{t}_{\mathrm{sig}}$, analogous to the strategy adopted to derive the final discriminant in the $\not\!\!E_T b\bar{b}$ s-channel single top search [9].

The s-channel optimized $\mathrm{NN}_{\mathrm{sig}}$ discriminant as used in the $\not\!\!E_T b\bar{b}$ s-channel electroweak single top search [9] and the $\mathrm{NN}^{t}_{\mathrm{sig}}$ discriminant of this analysis are combined to obtain an $\mathrm{NN}^{s+t}_{\mathrm{sig}}$ final discriminant, used to simultaneously separate both s- and t-channel signal processes from the remaining background. For events with $\mathrm{NN}_{\mathrm{sig}}$ outputs larger than 0.6, $\mathrm{NN}^{s+t}_{\mathrm{sig}}$ is defined to be equal to the $\mathrm{NN}_{\mathrm{sig}}$ output. For those events that do not satisfy the requirement on $\mathrm{NN}_{\mathrm{sig}}$, $\mathrm{NN}^{s+t}_{\mathrm{sig}}$ is defined as the $\mathrm{NN}^{t}_{\mathrm{sig}}$ output multiplied by 0.6. Figure 1 shows the predicted and observed shapes of $\mathrm{NN}^{s+t}_{\mathrm{sig}}$ output variable for each of the six event subsamples used in this analysis.

Several sources of systematic uncertainty are taken into account in this analysis. Uncertainties on assumed cross section values range from 5%-6% on $t\bar{t}$, VV (6%), VH (5%), $W+c$ (23%) cross sections [19–22]. Other systematic uncertainties arise from the normalization of the V-plus-heavy-flavor (30%) and of the MJ (3%-7%) background contributions. All samples whose normalizations are not constrained according to the data are subject to a luminosity uncertainty of 6% [23]. Furthermore, uncertainties are assigned due to the efficiencies of the lepton vetoes (2%). We also assign a normalization uncertainty of 2% due to variations in the assumed parton distribution functions. To account for differences in the trigger efficiency in data and simulation, a 2% rate uncertainty is assigned.

Possible mismodeling in the b-tagging efficiency is taken into account by applying scale factors to the simulation to correct its b-tagging efficiency to that of data. The scale factors vary depending on the tag category (all are on the order of unity), and the associated uncertainties range from 8%-16% [13]. Mistag rate uncertainties (20%-30%) are also included [13].

TABLE I: Numbers of predicted and observed events in the two-jet signal region in the subsample with exactly one tightly tagged jet (1T), one tightly and one loosely tagged jet (TL) and two tightly tagged jets (TT). The uncertainties in the predicted numbers of events are due to the theoretical cross section uncertainties and to the uncertainties on signal and background modeling. Both the uncertainties and the central values are those returned by the fit to the data with theory constraints.

Category	1T	TL	TT
$t\bar{t}$	243 ± 24	85 ± 9	92 ± 8
Diboson	285 ± 2	51 ± 1	37 ± 1
VH	17 ± 1	7 ± 1	8 ± 1
V+jets	6528 ± 2048	694 ± 216	220 ± 69
MJ	8322 ± 180	928 ± 59	300 ± 32
t-ch single top	160 ± 31	11 ± 2	9 ± 12
s-ch single top	86 ± 48	42 ± 23	46 ± 25
Total prediction	15557 ± 2056	1733 ± 224	663 ± 76
Observed	15312	1743	686

TABLE II: Numbers of predicted and observed events in the three-jet signal region in the subsample with exactly one tightly tagged jet (1T), one tightly and one loosely tagged jet (TL) and two tightly tagged jets (TT). The uncertainties in the predicted numbers of events are due to the theoretical cross section uncertainties and to the uncertainties on signal and background modeling. Both the uncertainties and the central values are those returned by the fit to the data with theory constraints.

Category	1T	TL	TT
$t\bar{t}$	597 ± 60	117.5 ± 13	110 ± 10
Diboson	108 ± 1	15.7 ± 0	9 ± 0
VH	6 ± 1	1.9 ± 0	2 ± 0
V+jets	1610 ± 505	164.5 ± 51	50 ± 16
MJ	1818 ± 49	187.5 ± 14	56 ± 8
t-ch single top	82 ± 16	8 ± 2	7 ± 1
s-ch single top	46 ± 25	15 ± 8	16 ± 9
Total prediction	4220 ± 511	495 ± 55	234 ± 20
Observed	4198	490	237

Uncertainties in the jet energy scale [11] are included by correlating the uncertainties in the predicted yields of signals and backgrounds (of the order of 1%-6%) with the corresponding distortions in the predicted kinematic distributions arising from jet energy scale shifts in all samples except the MJ background, which is entirely data-determined. An additional shape systematic uncertainty is incorporated for the MJ model, accounting for shape

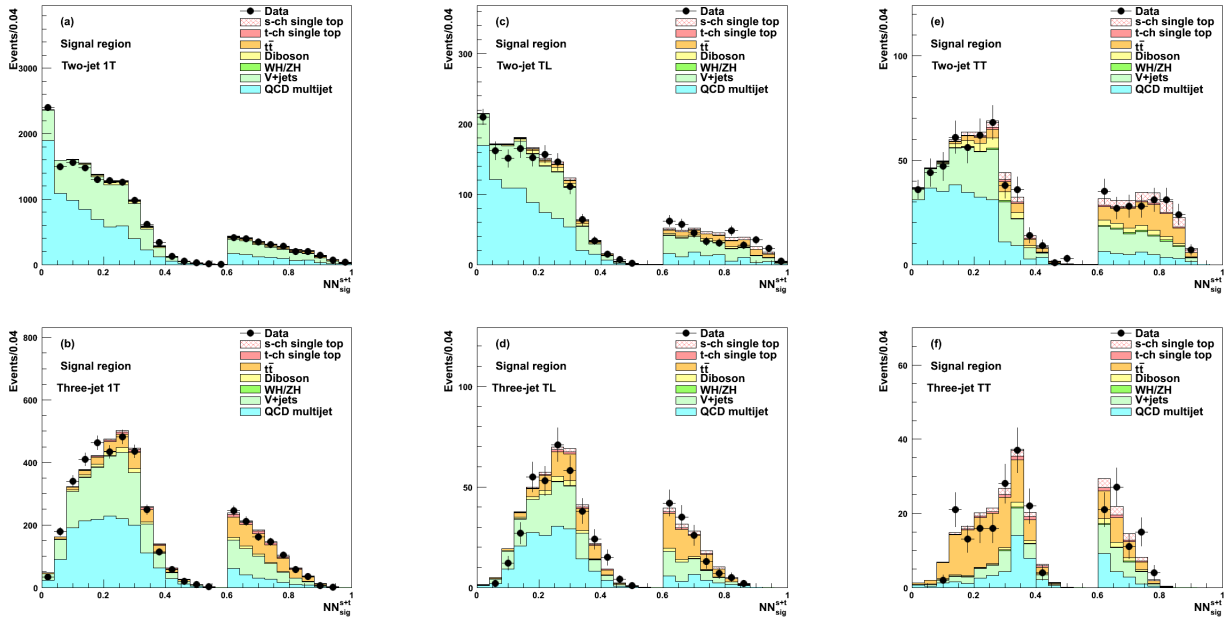

FIG. 1: Predicted and observed $\mathrm{NN}^{s+t}_{\mathrm{sig}}$ distributions in the signal region, for the (a) 1T two-jet, (b) 1T three-jet, (c) TL two-jet, (d) TL three-jet, (e) TT two-jet, (f) and TT three-jet subsamples.

variations in the MJ prediction.

To measure the electroweak single top production cross section, a combined likelihood is formed, which is the product of Poisson probabilities for each bin of the six $\mathrm{NN}^{s+t}_{\mathrm{sig}}$ discriminants shown in Fig. 1. To account for systematic uncertainties, a Bayesian technique is used, in which each independent source of systematic uncertainty is assigned a nuisance parameter with a Gaussian prior probability distribution. The impact of each nuisance parameter is propagated to the predictions of the signal and background yields in each bin of each histogram in the analysis. A non-negative uniform prior probability distribution is assumed for the single-top cross section, which is extracted from its posterior probability density after integrating over all nuisance parameters. After applying the measurement procedure on data, the obtained electroweak single top quark production cross section is $3.53^{+1.25}_{-1.16}$ pb, consistent with the SM prediction. The magnitude of V_{tb} is extracted from the posterior probability density by $|V_{tb}|^2_{\mathrm{obs}} = |V_{tb}|^2_{\mathrm{SM}}\sigma^{s+t}_{\mathrm{obs}}/\sigma^{s+t}_{\mathrm{SM}}$ assuming $|V_{tb}|^2_{\mathrm{SM}}$ is unity and by fixing the s- and t-channel relative contributions to their SM prediction. Including the theoretical uncertainty of the signal cross section (5.8% for s-channel, 6.2% for t-channel) [3] and assuming a uniform prior of $0 < |V_{tb}| < 1$, the magnitude is measured to be $|V_{tb}| > 0.63$ at the 95% credibility level (C.L.).

These results are combined with the results of the most recent CDF measurement of electroweak single top quark production in the $\ell\nu b\bar{b}$ sample, performed with 7.5 fb^{-1} as described in Ref. [10]. In this analysis, candidate events were selected by requiring exactly one reconstructed charged lepton (e or μ) in the final state. Hence, no such events are included in the $\not\!\!E_T b\bar{b}$ analysis described above. Four independent subsamples are formed based on the number of b-tagged jets using the SecVtx algorithm, and also the total number of jets: two jets and one b-tag, two jets and two b-tags, three jets and one b-tag, or three jets and two b-tags. Events were also divided into independent categories based on different lepton reconstruction algorithms. To further discriminate the signal from all other backgrounds, multivariate discriminants (NNs) were employed. These NNs were optimized separately for each of the four event subsamples. Correlated systematic errors were treated as described above for the $\not\!\!E_T b\bar{b}$ analysis. Finally, a Bayesian binned-likelihood technique was applied to the final NN output to extract an electroweak single top quark cross section of $3.04^{+0.57}_{-0.53}$ pb, assuming a top-quark mass of 172.5 GeV/c^2. The magnitude of V_{tb} was estimated following the same prescription described above and constrained to be $|V_{tb}| > 0.86$ at the 95% C.L.

The results of the two analyses are combined by taking the product of their likelihoods and simultaneously varying the correlated uncertainties, following the procedure explained above. The uncertainties associated with the theoretical cross sections of the $t\bar{t}$, VV, and VH production processes, and those associated with the luminosity are taken as fully correlated between the two analyses. The combined measurement results in an electroweak single top quark production cross section of $3.02^{+0.49}_{-0.48}$ pb, consistent with the SM prediction. The s- and t-channel cross sections are also extracted separately by constraining the other opposite-channel cross section to the SM prediction. The result is shown in Fig. 2a. From the posterior probability density on $|V_{tb}|^2$, shown in Fig. 2b, a 95% C.L. lower limit of $|V_{tb}| > 0.84$ is obtained.

We thank the Fermilab staff and the technical staffs of the participating institutions for their vital contributions. This work was supported by the U.S. Department of Energy and National Science Foundation; the Italian Istituto Nazionale di Fisica Nucleare; the Ministry of Education, Culture, Sports, Science and Technology of Japan; the Natural Sciences and Engineering Research Council of Canada; the National Science Council of the Republic of China; the Swiss National Science Foundation; the A.P. Sloan Foundation; the Bundesmin-

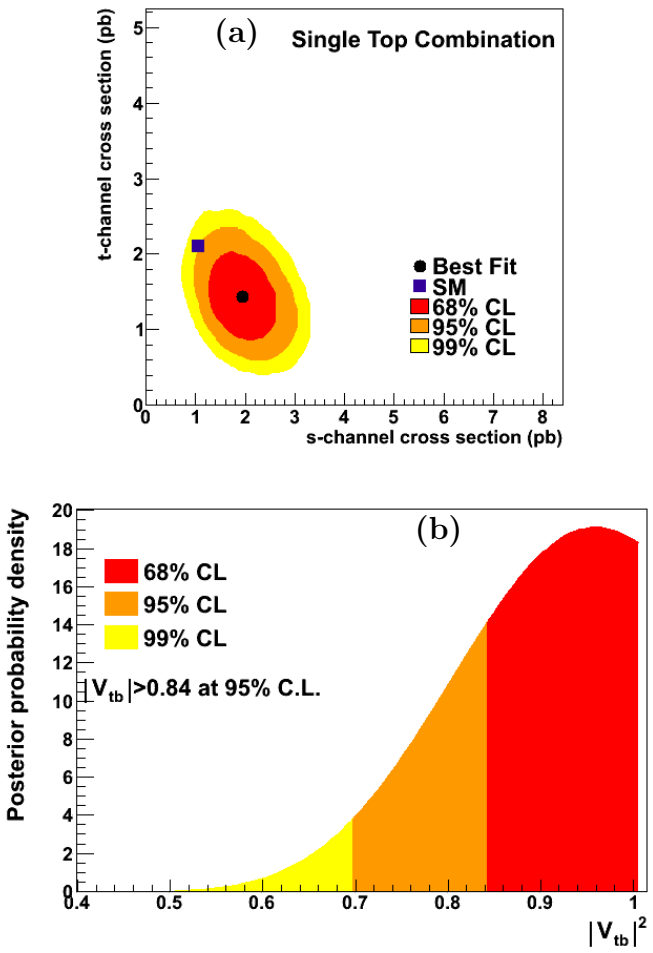

FIG. 2: CDF single-top combinations of the (a) two-dimensional posterior density of the measured s-vs.-t-channel cross sections, normalized to the SM predictions, and (b) the posterior probability density on $|V_{tb}|^2$, assuming the SM prediction for the relative contributions between the s- and t-channel processes.

isterium für Bildung und Forschung, Germany; the Korean World Class University Program, the National Research Foundation of Korea; the Science and Technology Facilities Council and the Royal Society, UK; the Russian Foundation for Basic Research; the Ministerio de Ciencia e Innovación, and Programa Consolider-Ingenio 2010, Spain; the Slovak R&D Agency; the Academy of Finland; the Australian Research Council (ARC); and the EU

community Marie Curie Fellowship contract 302103.

---

[1] V. M. Abazov *et al.* (D0 Collaboration), Phys. Rev. Lett. **103**, 092001 (2009); T. Aaltonen *et al.* (CDF Collaboration), Phys. Rev. Lett. **103** 092002 (2009).

[2] N. Cabibbo, Phys. Rev. Lett. **10**, 531 (1963); M. Kobayashi and T. Maskawa, Prog. Theor. Phys. 49, 652 (1973).

[3] N. Kidonakis, Phys. Rev. D **81**, 054028 (2010); **83**, 091503(R) (2011).

[4] Charge-conjugate processes are assumed throughout.

[5] N. Kidonakis, Phys. Rev. D **74**, 114012 (2006).

[6] We assume a branching ratio of 100% for $t \to Wb$.

[7] The calorimeter missing transverse energy $\vec{\not\!\!E}_T$(cal) is defined by the sum over calorimeter towers, $\vec{\not\!\!E}_T(\text{cal}) = -\sum_i E_T^i \hat{n}_i$, where i is a calorimeter tower number with $|\eta| < 3.6$, $\hat{n}_i$ is a unit vector perpendicular to the beam axis and pointing at the ith calorimeter tower. The reconstructed missing transverse energy, $\vec{\not\!\!E}_T$, is derived by subtracting from $\vec{\not\!\!E}_T$(cal) components of the event not registered by the calorimeter, such as jet energy adjustments. $\not\!\!E_T$ [$\not\!\!E_T$(cal)] is the scalar magnitude of $\vec{\not\!\!E}_T$ [$\vec{\not\!\!E}_T$(cal)].

[8] T. Aaltonen *et al.* (CDF Collaboration), Phys. Rev. D **81**, 072003 (2010).

[9] T. Aaltonen *et al.* (CDF Collaboration), To be published.

[10] T. Aaltonen *et al.* (CDF Collaboration), To be published.

[11] A. Bhatti *et al.*, Nucl. Instrum. Methods A 566 (2006) 375.

[12] C. Adloff *et al.* (H1 collaboration), Z. Phys. C 74 (1997) 221.

[13] J. Freeman, T. Junk, M. Kirby, Y. Oksuzian, T. J. Phillips, F. D. Snider, M. Trovato, J. Vizan, and W. M. Yao, Nucl. Instrum. Methods Phys. Res., Sect. A **697**, 64 (2013).

[14] S. Alioli *et al.*, J. High Energy Phys. 06 (2010) 043.

[15] M. L. Mangano, M. Moretti, F. Piccinini, R. Pittau, and A. D. Polosa, J. High Energy Phys. 07 (2003) 001.

[16] T. Sjöstrand, S. Mrenna, and P. Skands, J. High Energy Phys. 05 (2006) 026.

[17] D. Acosta *et al.* (CDF Collaboration), Phys. Rev. D **71**, 052003 (2005); A. Abulencia *et al.* (CDF Collaboration), Phys. Rev. D **74**, 072006 (2006).

[18] T. Aaltonen *et al.* (CDF Collaboration), Phys. Rev. D **87**, 052008 (2013).

[19] P. Baernreuther, M. Czakon and A. Mitov, Phys. Rev. Lett. **109**, 132001 (2012).

[20] J. M. Campbell and R. K. Ellis, Phys. Rev. D **60**, 113006 (1999).

[21] J. Baglio and A. Djouadi, J. High Energy Phys. 10 (2010) 064; O. Brien, R. V. Harlander, M. Weisemann, and T. Zirke, Eur. Phys. J. C **72**, 1868 (2012).

[22] T. Aaltonen *et al.* (CDF Collaboration), Phys. Rev. Lett. **110**, 071801 (2013).

[23] S. Klimenko, J. Konigsberg, and T. M. Liss, Report No. FERMILAB-FN-0741 (2003).